Localized magnetic moments on chromium and manganese dopant atoms in niobium and vanadium

A. Roy, D. S. Buchanan,* D. J. Holmgren, and D. M. Ginsberg
Department of Physics and Materials Research Laboratory, University of Illinois at Urbana—Champaign, 1110 West Green Street, Urbana, Illinois 61801
(Received 26 July 1984)

We have made magnetic susceptibility measurements on films of Nb and V, pure and doped with Cr and Mn. The results indicate the presence of localized moments on Cr and Mn dopant atoms in both Nb and V. We discuss the data in terms of a model which takes the magnetic behavior of the host metals into account. We have also measured the superconducting transition temperature, T_c, and the upper critical magnetic field, $H_{c2}(T)$, of several Nb films, pure and doped with Cr and Mn. We find that T_c of Nb is decreased in the presence of Cr or Mn, by amounts that are consistent with the existence of localized moments. The results for $H_{c2}(T)$ indicate, for both Cr and Mn dopants in Nb, that the pair-breaking effect of the magnetic dopants is additive with that of the applied magnetic field.

I. INTRODUCTION

When magnetic dopant atoms from among the $3d$ elements of the Periodic Table are put into transition-metal superconductor hosts, the effects of doping are interesting, both in the context of localized-moment formation and in the context of the pair-breaking effects of these atoms on the superconductivity of the hosts. Two factors are believed to inhibit the formation of localized moments on $3d$ dopants in these host metals:[1–4] the transition-metal superconductors have a characteristically large density of electronic states at the Fermi level, and $3d$ magnetic dopants interact strongly with the conduction electrons of the host metal. (The strength of the exchange interaction is on the order of 1 eV for $3d$ magnetic dopants, as, for example, compared with ~ 0.1 eV for $4f$ dopants.[5]) Nevertheless, localized moments do exist on $3d$ dopants in a number of transition-metal superconductors (a listing is provided in Ref. 6). It is not possible, on the basis of current theories, to make quantitatively reliable predictions regarding any particular dopant-host system,[5,7–10] so each case of interest must be investigated experimentally. If localized moments are present, the large density of electronic states at the Fermi level tends to diminish the pair-breaking effects associated with these moments, while the strong exchange interaction of the dopant atoms with the conduction electrons tends to enhance those effects.[11–13]

We have investigated the possibility that Cr and Mn dopant atoms have localized moments when present in low concentrations in Nb and V. We did this by means of static susceptibility measurements on films of the pure and doped materials, in conjunction with tunneling measurements.[14] As we will see, one must take the magnetic behavior of the host into account to explain our results. Otherwise one would be led to believe, incorrectly, that there are only small localized moments on Cr and Mn in Nb and on Cr in V, and one would not be able to understand the V-Mn results at all. We will show that our results can be understood in terms of a model which includes the interactions of the dopant moment with both the conduction electrons and local moments on the host atoms. We also present a simple calculation of the dopants' contribution to the susceptibility, based on our model.

Previous experiments to detect the presence of localized moments on Cr and Mn dopants in Nb and V have been inconclusive. Barton and Claus[15] measured the susceptibilities of pure Nb and of Nb doped dilutely with Cr and Mn. They concluded that local moments do not exist on Cr or Mn in Nb. Our experimental results, however, show that their measurement technique lacked the required sensitivity. Müller[16] studied the depression of the superconducting transition temperature of V, which is caused by Cr and Mn dopants, and concluded that both Cr and Mn are magnetic in V. However, this conclusion was questioned by Gladstone *et al.*,[17] who contended, on the basis of the rigid-band model, that the observed T_c depression could be accounted for without invoking the presence of localized moments.

In order to investigate the pair-breaking effects associated with these $3d$ dopants in a transition-metal superconductor, we measured the transition temperature T_c and the upper critical field, $H_{c2}(T)$, of films of Nb, pure and doped with Cr and Mn. As we will see, T_c of Nb is decreased by Cr or Mn dopants, by amounts that are consistent with the predictions of band calculations[13] and the theory of Shiba[11] for magnetically doped superconductors. We will compare our results for $H_{c2}(T)$ with the additive pair-breaking theory of Fulde and Maki,[18] which predicts that the pair-breaking effects of the magnetic dopants and of the applied magnetic field are additive, and that the pair-breaking effect of the magnetic dopants is independent of temperature.

II. EXPERIMENTAL DETAILS

A. Magnetic susceptibility measurements

The samples used for the magnetic susceptibility measurements were films of Nb and V, pure and doped with

Cr and Mn. They were made by coevaporation onto substrates in the ultrahigh-vacuum chamber of a molecular-beam epitaxy facility. The starting materials and known impurities expressed in atomic percent (at.%) were the following: Nb (99.99% pure, except for a Ta concentration of 0.018 at.%); V (99.95% pure); Cr (99.999% pure); and Mn (99.99% pure). All the samples were deposited in background pressures between 5×10^{-9} and 1×10^{-8} Torr. The Nb was deposited at rates of 1.5—2.0 Å/sec, and the V at about 10 Å/sec. The dopants were deposited simultaneously at rates calculated to yield the desired doping concentration. The substrate temperature was held at 200 °C for each Nb sample, and at 800 °C for each V sample. Further details of the sample preparation procedure are described elsewhere.[14,19]

Characteristics of all the samples are listed in Table I (ppm denotes atomic parts per million). The substrates for the Nb samples were cut from 152-μm-thick slides of high-purity quartz. The Nb films were about 2.5-μm thick, with areas of approximately 0.4 cm^2. The V samples were grown epitaxially on sapphire substrates, which were cut from a single slide of 254-μm-thick z-cut sapphire. The V films were about 1.9 μm thick, with areas of approximately 0.5 cm^2. The dopant concentrations listed in Table I are nominal values, derived from the deposition procedures; we believe these values are accurate to within a factor of 2 (Ref. 14).

We measured the total magnetic moment of each sample, as a function of temperature in a SQUID (superconducting quantum interference device) susceptometer.[20] The quantity of interest for each dopant-host system was the temperature-dependent contribution of the dopant atoms. The Nb films had magnetic moments on the order of 2×10^{-9} emu per gauss of applied field. Superimposed on this was a temperature-dependent signal due in part to the Nb itself and in part to the signal arising from the dopant atoms. The total change in the dopant-atom signal in the entire temperature range of the investigation was comparable to the change in the Nb signal, on the order of 5×10^{-11} emu per gauss. To successfully identify the nature of the temperature dependence of the dopant-atoms' signal we therefore needed to measure the magnetic moments of our films to a precision of 10^{-12} emu per gauss. This is a factor of 10 below the noise level of the susceptometer, which is 10^{-11} emu per gauss. (For the V films these values are similar, except that the temperature-dependent part of the V signal was larger by a factor of about 6.)

A problem inherent in high-precision SQUID susceptometer measurements of small magnetic moments concerns the need for a suitable sample holder. The sample holder should have a magnetic moment which is small compared to that of the sample, yet it should be massive enough for satisfactory suspension using thread. We found that the sample-substrates themselves constituted the best sample holders for our films; high-purity quartz and sapphire are, in fact, two of the most desirable materials for use in sensitive magnetic measurement apparatus.[6,21] Although the magnetic moment of a quartz substrate was about 3 times that of a Nb film, and the magnetic moment of a sapphire substrate was about 5 times that of a V film, this was nevertheless an acceptable situation because we could remove each film from its substrate and then measure the substrate's moment in a reproducible way with the required precision of 1 part in 10^4. (This procedure also automatically canceled out the temperature-dependent signal[6,21] caused by the displaced background He gas.) Also, since the applied magnetic field in the susceptometer is oriented in the vertical direction, vertical suspension of the film on its substrate (using thread) results in a negligibly small demagnetization factor.[22] An additional concern related to sample holders is the need for an appropriate suspension material. We found that the cotton and polyester fibers commonly used by others as suspension materials were unsuitable for our purposes: These materials had large temperature-dependent paramagnetic susceptibilities at low temperatures, perhaps because of metallic contaminants introduced during the manufacturing process. We suspended our samples using fine silk thread which was unraveled from a piece of undyed Kashmir silk cloth. The silk was probably fabricated on wooden spindles because it was free of paramagnetic impurities and had the small diamagnetic susceptibility characteristic of an organic material. This thread had a magnetic moment of -1.5×10^{-11} emu per gauss per centimeter of length.

It is difficult, using a SQUID susceptometer, to obtain data that are reproducible to 1 part in 10^4 at a level of precision which is an order of magnitude below the noise level. Even after minimizing the effects of the various noise sources, the reproducibility of the measurements depends critically on the behavior of the superconducting differential shield and the density of the He gas in the sample region. We developed a set of procedures for obtaining data reproducible to better than 1 part in 10^4. These procedures are described in Refs. 6 and 21.

TABLE I. Characteristics of the samples used for the susceptibility measurements.

Sample no.	Constituents	Dopant concentration (ppm)	Volume (10^{-4} cm^3) ±0.08%	Substrate mass (mg) ±0.001 mg
Nb-1	Nb		0.9981	17.390
Nb-2	Nb-Cr	400	1.0538	16.052
Nb-3	Nb-Mn	460	0.9186	17.639
V-1	V		0.8708	54.548
V-2	V-Cr	480	0.8825	55.256
V-3	V-Mn	510	0.9271	55.787

All the magnetic moment measurements were carried out in an applied field of 20 kG. This value was chosen in order to provide access to temperatures well below the superconducting transition temperature of Nb. (The H_{c2} measurements show that our evaporated Nb films are in the normal state down to a temperature of 6 K at 20 kG.) After the total magnetic moment of each sample on its substrate was measured at various temperatures, the film was etched off the substrate, and the substrate moment was measured at the same temperatures. We made 200 to 300 readings at each temperature point to average out instrument noise and the effect of temperature fluctuations. The magnetic moment of the film was then determined by subtracting the substrate's moment from the total moment. Finally, the contribution due to the dopant atoms, for each dopant-host system, was found by subtracting the magnetic moment of the pure film from that of the doped one, using appropriate scale factors to account for different sample sizes.

The scale factors consisted of the volume of each film and the mass of each substrate before and after the film was etched off. The area of each film was determined by using a planimeter to measure the area of a magnified (about 250×) image of the film, and the thickness was measured with a Tencor Alpha-step profiler. Values of 8.4 g/cm^3 for the density of Nb and 6.1 g/cm^3 for V (Ref. 23) were then used to find the mass of each film from its volume. The relative uncertainty in the measurement of the volumes (masses) of the films by this procedure was typically less than 0.08% (0.6 μg). Although small, this proved to be the largest source of systematic error in the experiment. The mass of each substrate was found by subtracting the mass of the film from that of the substrate with the film, measured on an electrobalance with an accuracy of 1 μg. Measurements of the masses of the substrates after removing the films showed that about 0.4% of the quartz and 0.02% of the sapphire substrates had been lost in the etching process.

B. Superconductivity measurements

The samples used for the superconductivity measurements were films of Nb, pure and doped with Cr and Mn. These films were deposited on glass substrates, and were made under the same conditions as the Nb films used for the susceptibility measurements. In order to facilitate the resistivity measurements, which were made with a four-probe dc technique, each sample film was deposited to an "S" pattern: This provided a film length of 6.36 cm between the voltage probes.

The width of each sample was 0.102 cm, and its thickness was measured with a Tencor Alpha-step profiler. The resistance of each sample was measured at room temperature ($R_{300\,K}$), and at a temperature ($\sim$9.5 K) just above the superconducting transition temperature ($R_{9.5\,K}$). The residual resistivity was obtained from $R_{9.5\,K}$, and the resistivity ratio was defined as $R_{300\,K}/R_{9.5\,K}$. The lattice parameter of each sample was determined by x-ray diffraction.

The transition temperature T_c was defined as the midpoint of the resistive transition, and the transition width δT_c was defined as the temperature interval between the 10% and 90% points of the transition.

Values of the upper critical field $H_{c2}(T)$ for each sample were determined by measuring the temperature of the superconducting transition as a function of applied field. The field was oriented perpendicular to the sample surface, and was generated by a superconducting solenoid capable of reaching 26 kG. The field was held fixed (with the solenoid in the persistent mode) at various applied-field values while the temperature was swept through the transition. The current densities used for the resistive transitions were typically between 2 and 6 A/cm^2.

Temperatures were measured with a germanium resistance thermometer which was also calibrated for use in magnetic fields of up to 26 kG. Temperature regulation was provided by an electronic temperature regulator, using a capacitance thermometer as the feedback element. Magnetic fields were measured with a Hall probe, which was calibrated for both field and temperature.[6]

III. RESULTS AND DISCUSSION

A. Magnetic susceptibility measurements

In the following, for each dopant-host system, the contribution of the dopant atoms to the volume susceptibility is denoted by χ_m, and is obtained by subtracting the susceptibility of the pure host metal from that of the doped sample.

1. Cr and Mn dopants in Nb

Figure 1 shows a plot of χ_m vs $1/T$ for Cr dopants in Nb. It can be seen from this figure that, within random uncertainties, χ_m increases linearly with $1/T$. This indicates that χ_m obeys a Curie law, which, following the usual interpretation of a static susceptibility measurement, implies that a localized moment is present on each Cr

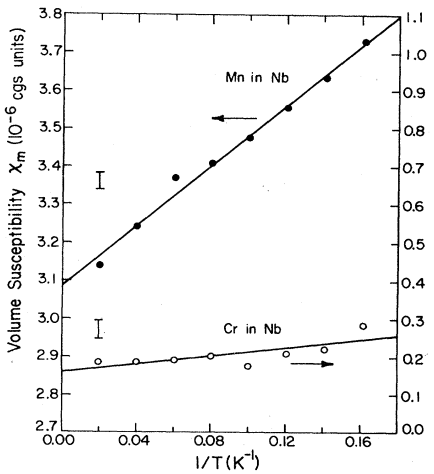

FIG. 1. Open and solid circles: the contribution of Cr dopants (400 ppm) and Mn dopants (460 ppm) to the volume susceptibility of Nb, respectively. The error bars correspond to a magnetic moment uncertainty of $\pm 2.4\times10^{-12}$ and $\pm 2.2\times10^{-12}$ emu per gauss, respectively.

atom in Nb. We fit the data to a Curie law of the usual form,

$$\chi_m = \chi_0 + \frac{n_m \mu_B^2 P_m^2}{3 k_B T} , \tag{1}$$

where n_m is the concentration of dopant atoms and P_m is the effective number of Bohr magnetons μ_B per dopant atom. This fit yields (for Nb-Cr)

$$P_m = (0.34 \pm 0.06)\mu_B/\text{atom} ,$$
$$\chi_0 = (0.16 \pm 0.10) \times 10^{-6} \text{ cgs units} . \tag{2}$$

A plot of χ_m vs $1/T$ for Mn in Nb is also shown in Fig. 1. χ_m is evidently a linear function of $1/T$: A fit to Eq. (1) yields (for Nb-Mn)

$$P_m = (0.86 \pm 0.02)\mu_B/\text{atom} ,$$
$$\chi_0 = (3.09 \pm 0.10) \times 10^{-6} \text{ cgs units} . \tag{3}$$

In each plot in Fig. 1, the straight line is the least-squares best-fit line, and the error bar shows a typical uncertainty (plus or minus one standard deviation) in any value of χ_m caused by random errors. (The error bars correspond to a magnetic moment uncertainty of about $\pm 2.3 \times 10^{-12}$ emu per gauss.)

2. *Cr and Mn dopants in V*

A plot of χ_m vs $1/T$ for Cr in V is shown in Fig. 2. The data point at 50 K ($1/T = 0.02$) clearly falls outside the scatter in the rest of the data, probably because of an experimental error: nonequilibrium of the susceptometer during the measurement of the magnetic moment of a substrate. Omitting the 50-K point from the analysis, we fit the remaining data to the Curie law of Eq. (1) to obtain (for V-Cr)

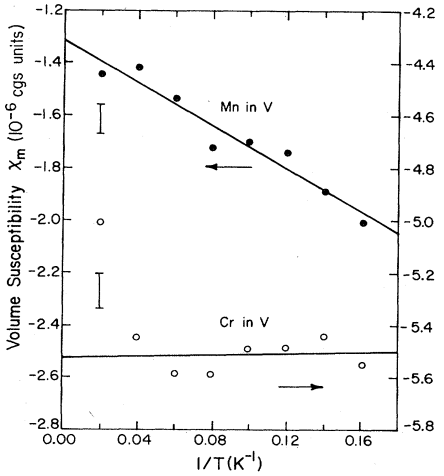

FIG. 2. Open and solid circles: the contribution of Cr dopants (480 ppm) and Mn dopants (510 ppm) to the volume susceptibility of V, respectively. The error bars correspond to a magnetic moment uncertainty of $\pm 5.9 \times 10^{-12}$ and $\pm 4.9 \times 10^{-12}$ emu per gauss, respectively. The data point at 50 K ($1/T = 0.02$) for Cr doping is believed to be in error, and has been omitted from the analysis.

$$P_m = (0.14 \pm 0.36)\mu_B/\text{atom} ,$$
$$\chi_0 = (-5.53 \pm 0.21) \times 10^{-6} \text{ cgs units} . \tag{4}$$

Figure 2 also shows a plot of χ_m vs $1/T$ for Mn in V. χ_m is evidently linear in $1/T$; however, the slope of the χ_m-vs-$1/T$ line is negative. Although this is certainly not Curie-law behavior in the usual sense, we can obtain an estimate of the magnitude of the effect by fitting the data to

$$\chi_m = \chi_0 - \frac{n_m \mu_B^2 (P_m')^2}{3 k_B T} .$$

We get (for V-Mn)

$$P_m' = (0.73 \pm 0.04)\mu_B/\text{atom} ,$$
$$\chi_0 = (-1.32 \pm 0.25) \times 10^{-6} \text{ cgs units} . \tag{5}$$

In each plot in Fig. 2, the straight line is the least-squares best-fit line, and the error bar shows a typical random uncertainty in any value of χ_m. (The error bars correspond to a magnetic moment uncertainty of about $\pm 5.4 \times 10^{-12}$ emu per gauss.)

The indicated uncertainties in the values of P_m and χ_0 in Eqs. (2)—(5) were estimated by procedures described in Ref. 6. The uncertainty in each value of P_m is essentially a reflection of the random errors, while the uncertainties in χ_0 reflect the comparatively large possible systematic errors in the experiment. We have excluded uncertainties in the values of n_m: The indicated uncertainties in P_m are therefore a measure only of the precision of our susceptibility measurements. Including uncertainties in n_m, we believe that our values for P_m are accurate to only $\pm 50\%$.

In a traditional sense, our results indicate the presence of localized magnetic moments on Cr and Mn dopant atoms in Nb and on Cr dopant atoms in V. This follows from the observed Curie-law behavior of χ_m for each of these dopant-host systems. Our results for the V-Mn system, however, cannot be explained on the basis of traditional models, and we cannot make a corresponding statement regarding the presence of localized moments on Mn dopant atoms in V. Nonetheless, the observed linear decrease of χ_m as a function of $1/T$ for the V-Mn system is at least suggestive of the presence of localized states (virtual bound states or bound states) in the system.

3. *A theoretical model*

In order to understand the behavior of the V-Mn system and to account for the relatively small values of P_m associated with the dopants in the Nb-Cr, Nb-Mn, and V-Cr systems, we first consider our results for the susceptibility χ_h of each host metal.

Figure 3 shows plots of χ_h vs T for our pure Nb and pure V films. χ_h for each host-metal film is a decreasing function of temperature, changing by 1.3% between 6.2 and 50 K for Nb, and by 3.6% for V. The temperature dependence of the susceptibility of transition metals like Nb or V is usually ascribed to the temperature dependence of the Pauli paramagnetism of the conduction electrons, caused by the strong energy dependence of the density of electronic states of Nb and V in the neighborhood of the Fermi level.[24,25] The temperature dependence of the Pauli

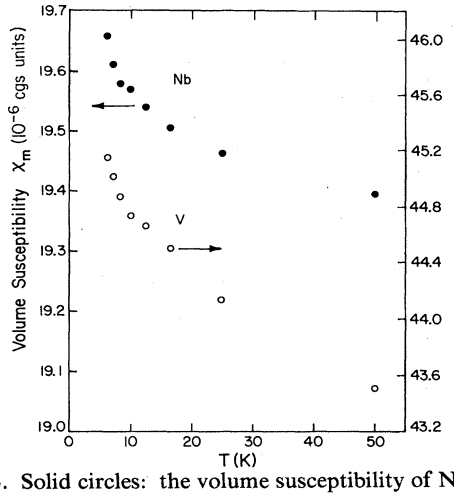

FIG. 3. Solid circles: the volume susceptibility of Nb (sample Nb-1) vs temperature. Open circles: the volume susceptibility of V (sample V-1) vs temperature.

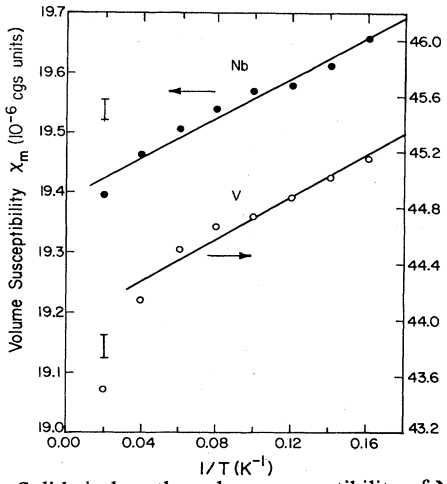

FIG. 4. Solid circles: the volume susceptibility of Nb (sample Nb-1) vs $1/T$. Open circles: the volume susceptibility of V (sample V-1) vs $1/T$. The data point at 50 K ($1/T=0.02$) has been excluded from the calculation of the least-squares best-fit line.

paramagnetic susceptibility χ_p is expressed (correct to second order in T) by[26]

$$\chi_p(T)=\mu_B^2 g(\epsilon_F)\left\{1-\frac{\pi^2 k_B^2}{6}T^2\left[\left[\frac{g'}{g}\right]^2-\frac{g''}{g}\right]\right\}, \quad (6)$$

where the density of states $g(\epsilon)$ and its derivatives g' and g'' are all evaluated at ϵ_F, the Fermi level at $T=0$. The effects of g' and g'' on $\chi_h(T)$ for Nb and V which would be predicted by Eq. (6) do not agree with the observed temperature dependence: a positive curvature at low temperatures and a decrease at higher temperatures, so we surmise that the main features of $\chi_h(T)$ are not determined by g' and g''. To be more quantitative, we need an estimate of the size of the effect. This may be obtained for Nb by using values of g and g' derived from a band-structure calculation of the density of states by Mattheiss.[24] We get $g(\epsilon_F)=6.6\times10^{34}$ states $\text{erg}^{-1}\,\text{cm}^{-3}$ and $g'(\epsilon_F)\simeq-1.1\times10^{47}$ states $\text{erg}^{-2}\,\text{cm}^{-3}$. It is difficult to obtain g'' from the calculation. We assume $g''=0$ and we use Eq. (6) to calculate the expected change in the susceptibility, $\Delta\chi=\chi_p(6.2)-\chi_p(50.0)$. We find $\Delta\chi\simeq1.2\times10^{-9}$ cgs, which is smaller than the observed change in $\chi_h(T)$ by a factor of about 200. A similar calculation for V, using the values $g(\epsilon_F)=8.9\times10^{34}$ states $\text{erg}^{-1}\,\text{cm}^{-3}$ and $g'(\epsilon_F)\simeq-7.3\times10^{46}$ states $\text{erg}^{-2}\,\text{cm}^{-3}$ derived from Ref. 25, shows that the expected change in $\chi_h(T)$ is smaller than the observed change by a factor of about 4000. We conclude that the effect of the energy dependence of the density of states is negligible for both pure films.

Figure 4 shows the susceptibility data for the pure films, plotted as a function of $1/T$. As is evident from Fig. 4, χ_h for Nb is nearly linear in $1/T$ within the temperature range of our investigation. For V, χ_h vs $1/T$ shows linear behavior below 16.5 K (i.e., for $1/T$ above 0.061). Above 16.5 K, the data have an increasing slope. We believe that this curvature can be ascribed to a real effect rather than to an artifact of the measurements. This temperature dependence of χ_h for each pure film may arise from effects associated with thermal expansion of the film (and/or differential thermal expansion between the film and the substrate) or from enhancement effects due to spin fluctuations, which are important in Nb and V (Ref. 27). However, the Curie-type behavior of χ_h for Nb (and, below 16.5 K, for V) suggests a simpler explanation—that localized moments are present in each pure host metal. This conclusion is not inconsistent with measurements of the temperature variation of the Knight shift in these metals.[28] (In this context, keeping in mind that crystalline order plays an important role in determining the magnetic behavior of transition metals,[10] we suggest that Knight-shift measurements be made on films of Nb and V, evaporated under conditions similar to ours.)

Invoking the presence of localized moments in each pure host metal enables a simple treatment of the effects of the host-metal magnetism on the susceptibility of the dopant atoms in terms of a model which assumes that a localized moment is present on each atom of each host metal. The temperature dependence of $\chi_h(T)$ can then be attributed to the Curie susceptibility of these local moments, as modified by interactions with each other, and with the conduction electrons. For Nb, we can find an effective Bohr magneton number for each Nb moment by fitting the data for the pure film to

$$\chi_h=\chi_{h0}+\frac{n_h\mu_B^2 P_h^2}{3k_B T}, \quad (7)$$

where n_h is the concentration of host atoms. We obtain $P_h=(0.012\pm0.0005)\,\mu_B$/atom. The straight line in Fig. 4 is the least-squares best-fit line. We do not have an explanation for the deviation of the V data from a straight line at the higher temperatures. Omitting the highest temperature (50-K) data point, we fit the remaining data to Eq. (7) to obtain $P_h=(0.024\pm0.001)\mu_B$/atom. The higher-temperature ($1/T\leq0.061$) data correspond to $P_h=0.048\mu_B$/atom: We conclude that the local moment on each V atom has an effective Bohr magneton number of at least 0.024. The straight line in Fig. 4 is the least-

squares best-fit line calculated excluding the data point at 50 K.

We assume in this model that a localized magnetic moment exists on each dopant atom in the metallic host. The dopant atom interacts with the conduction electrons and the host atoms in its local environment via exchange interactions. The effects of these two exchange interactions can be pictured, in a mean-field theory, in terms of exchange fields, which can add to or subtract from an external applied field. In this picture, the response of the doped system to an external field is actually its response to a combination of external and exchange fields. In interpreting a static susceptibility measurement, one subtracts the response of the host system (host atoms and conduction electrons) from that of the doped system. The result of analyzing such measurements is therefore the response of the dopant atoms to the combination of external and exchange fields and the response of the host atoms and conduction electrons to the exchange fields alone. This result can be very different from the response of the dopant atoms to a purely external field.

In terms of this model, we can interpret our results for the V-Mn system as possibly corresponding to the case when either or both the interactions are antiferromagnetic. The low values of P_m for our other systems can conceivably be accounted for on a similar basis. To put these ideas on a more quantitative level, we performed a simple mean-field calculation of the magnetic susceptibility based on this model.[6] We present here only the assumptions and predictions of this calculation. We make the following assumptions.

(i) The dopant atoms do not interact with each other, and they respond independently to the combined external and exchange fields. This is justified because, at a doping level of 500 ppm in Nb or V, the dopants are on the average separated by 10 lattice spacings. [This value is obtained from $(n_m)^{-1/3}$.] Each dopant atom has a local moment with an effective Bohr magneton number which we call P_m.

(ii) The interactions of the host atoms with each other and with the conduction electrons are taken into account by assuming that the host-atom susceptibility follows a Curie-Weiss law $[1/(T-\Theta)]$ with an effective Bohr magneton number per host atom which we call P_h.

(iii) The conduction electrons are Pauli paramagnetic in the combined external and exchange fields ($\chi_p = n_e\mu_B^2/k_BT_F$, where n_e is the conduction-electron concentration and T_F is the Fermi temperature).

(iv) Temperature-independent diamagnetic terms are neglected; we assume that they will cancel out on subtracting the host system susceptibility from that of the doped system.

The model Hamiltonian for the doped system in the presence of an external field is

$$H = H_n + H_{\text{int}} . \tag{8}$$

H_n is the Hamiltonian describing the individual responses of the dopant atoms, host atoms, and conduction electrons to only the external field. The interactions of the dopant atoms with the host atoms and the conduction electrons are contained in H_{int}, which is given by

$$H_{\text{int}} = -2J_1\mathbf{S}_m\cdot\mathbf{S}_h - 2J_2\mathbf{S}_m\cdot\mathbf{S}_e . \tag{9}$$

Here $\mathbf{S}_m$, $\mathbf{S}_h$, and $\mathbf{S}_e$ are the spins on the dopant atom, host atom, and conduction electron, respectively. J_1 is the exchange constant for the interaction between the dopant atoms and the host atoms, and J_2 is the exchange constant for the dopant-atom—conduction-electron interaction. [J_1 and J_2 actually depend on the distance R between two interacting spins. We are making the approximation that $J(R)$ can be described by a step function: $J(R)=0$ for $R > V^{1/3}$, where V is a volume on the order of that for a unit cell of the host lattice.] We write H_{int} in the "Ising" form and employ a self-consistent mean-field approximation to determine the susceptibility of the doped system, χ_d. We then subtract the susceptibility of the host system from χ_d, obtaining the following expression for the "susceptibility of the dopant atoms,"

$$\chi_m^c = \frac{n_m\mu_B^2P_m^2}{3k_BT}\left[\frac{(1+A_1+A_2)^2}{1-A_1A_1'-A_2A_2'}\right], \tag{10}$$

where

$$A_1 = A_1(T) = \frac{J_1N_1P_h^2}{3k_Bg_1g_2(T-\Theta)} ,$$

$$A_2 = \frac{J_2N_2}{k_Bg_1g_3T_F} ,$$

$$A_1' = A_1'(T) = \frac{J_1N_1n_mP_m^2}{3k_Bn_hg_1g_2T} ,$$

$$A_2' = A_2'(T) = \frac{J_2N_2n_mP_m^2}{3k_Bn_eg_1g_3T} ,$$

and g_1, g_2, and g_3 are the g factors for the dopant atoms, host atoms, and conduction electrons, respectively. The parameters A_1 and A_1' both contain the factor J_1N_1, where N_1 is the number of host atoms that interact with each dopant atom. Because we assumed the exchange interaction has a short range, N_1 can be taken to be the number of nearest-neighbor host atoms in the case of substitutional doping. Thus, for a bcc host lattice (as in Nb and V), $N_1=8$. For interstitial dopants, a useful estimate of N_1 is the number of host atoms within the volume occupied by a unit cell. In this case, N_1 for a bcc host lattice will be somewhere higher than 8, let us say 9 or 10. Both A_2 and A_2' contain the factor J_2N_2, where N_2 is the average number of conduction electrons that interact with each dopant atom. The interpretation of N_2 is not as straightforward as that for N_1 because of the itinerant nature of the conduction electrons. We note, however, that the interaction between a dopant atom and the conduction electrons is actually an exchange interaction between the d electrons of the dopant atom and the conduction electrons predominantly in the d band of the host metal. We therefore replace J_2N_2 by $J_2\rho_dN_1$, where ρ_d is the number of filled d band electron states per atom. An estimate of ρ_d for the transition metals is given by

$$\rho_d = \frac{1}{n_h}\int_{\Delta_d} g(\epsilon)d\epsilon \simeq \frac{g(\epsilon_F)}{n_h}\Delta_d . \tag{11}$$

where $g(\epsilon_F)$ is the density of states at the Fermi level, and

Δ_d is the occupied width of the d band.

The predictions of our model calculation are contained in Eq. (10). The factor outside the large parentheses is just the Curie law for isolated dopant atoms. The expression within the large parentheses determines the apparent deviations from Curie-law behavior because of the interactions. These deviations depend on the temperature, primarily through the parameter A_1 (as can be seen by taking the $1/T$ factor inside the large parentheses). This shows that the temperature dependence of the deviations are a result of the temperature-dependent response of the host atoms to the exchange field.

To illustrate that our results for each dopant-host system could be accounted for on the basis of this model, we used a value of $P_m=4.9$ in Eq. (10) to evaluate χ_m^c as a function of $1/T$ for each system. This value of P_m, which corresponds to the ground state of Cr and Mn ions in the $3d^4$ configuration (assuming complete quenching of the orbital moment by the lattice crystalline field), was chosen mainly for the purpose of illustration. In the following, the dopants in each host are considered in turn.

4. $\chi_m^c(1/T)$ for Cr and Mn in Nb

We use the following values for the constants in Eq. (10) to evaluate $\chi_m^c(1/T)$ for Cr and Mn dopant atoms in Nb: $P_m=4.9$, $P_h=0.012$ (our experimentally observed value for Nb), $\Theta=0$ K, $k_BT_F=5.3$ eV (the free-electron value[29] for Nb), $g_1=g_2=g_3=2$, and n_m corresponding to 430 ppm (the average of the nominal concentrations for our Cr and Mn dopants in Nb. This value is reasonable, considering the uncertainty in the nominal concentrations.)

J_1N_1 and J_2N_2 are treated as adjustable parameters to fit $\chi_m^c(T)$ to $\chi_m(T)$ for each of the dopants. Only the temperature-dependent part of $\chi_m(T)$ is considered because of the large experimental uncertainties in the values of χ_0 and because our calculation does not take temperature-independent terms into account. Assuming that the interaction of the local moments with the conduction electrons is antiferromagnetic,[4] J_2N_2 is limited to negative values. Furthermore, for simplicity, the same value of J_2N_2 is used in the cases of both Cr and Mn.

We find that reasonably good fits to the data are obtained by using $J_2N_2=-210$ eV, with $J_1N_1=5.6$ eV for Cr, and $J_1N_1=42.0$ eV for Mn. The results are shown in Fig. 5. It should be pointed out here that these fits are not unique; we could get equally good fits by using higher values for $|J_2N_2|$. However, the corresponding numbers for J_1N_1 would also be higher: In this sense, we can regard the above-mentioned values for $|J_2N_2|$ and J_1N_1 as lower limits.

We can use these values of J_1N_1 to estimate the exchange constants J_1. Assuming interstitial doping, we set $N_1=10$ to obtain $J_1=0.6$ eV for Cr and $J_1=4.2$ eV for Mn, in Nb. To get an estimate for J_2, we replace J_2N_2 by $J_2N_1\rho_d$, where ρ_d is given by Eq. (11). We use the values $g(\epsilon_F)=26$ states/Ry atom and $\Delta_d=0.3$ Ry from Ref. 24 to get $\rho_d=7.8$ states/atom, from which we obtain $J_2=-2.7$ eV.

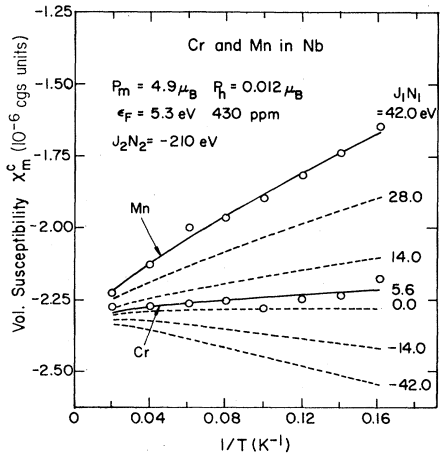

FIG. 5. Comparison of the susceptibility data with the results of the model calculation, for Cr and Mn dopants in Nb. The solid curves are plots of the calculated susceptibility $\chi_m^c(1/T)$ for Cr and Mn, and the circles represent the corresponding experimental values. The dashed curves are generated by using the values of J_1N_1 shown in the figure. Note that negative values of J_1 lead to negative slopes of $\chi_m^c(1/T)$.

5. $\chi_m^c(1/T)$ for Cr and Mn in V

To evaluate χ_m^c as a function of $1/T$ for Cr and Mn dopant atoms in V, we use the same parameters as in the case of Nb, except $P_h=0.024$ (our experimentally observed value for V), and n_m corresponding to 500 ppm (the average of the nominal concentrations for our Cr and Mn dopants in V).

Again, J_1N_1 and J_2N_2 are treated as adjustable parameters to fit $\chi_m^c(T)$ to $\chi_m(T)$ for each of the dopants. We find that reasonably good fits are obtained by using the same $J_2N_2=-210$ eV, with $J_1N_1=0.14$ eV for Cr, and $J_1N_1=-11.9$ eV for Mn. Figure 6 shows the results of the fitting procedure.

As shown in Fig. 6, the negative slope of $\chi_m(1/T)$ for Mn is easily accounted for on the basis of an antiferromagnetic interaction between the local moments on the Mn and V atoms. This is one of the most striking features of our model.

Estimates can be obtained for the exchange constants J_1 and J_2 by using the values found above for J_1N_1 and J_2N_2. Assuming substitutional doping, we set $N_1=8$ to obtain $J_1=0.02$ eV for Cr and $J_1=-1.5$ eV for Mn in V. To estimate J_2 we use the values $g(\epsilon_F)=26.6$ states/Ry atom and $\Delta_d=0.24$ Ry from Ref. 25 to obtain $\rho_d=6.4$ states/atom, from which we infer that $J_2=-4.1$ eV.

6. General remarks

It is seen from the foregoing results that satisfactory fits to the data for all the systems lead to reasonable values of J_1 and J_2. Therefore the experimental results are compatible with the presence of a local moment that could possibly be as large as $4.9\mu_B$ on each Cr and Mn dopant atom in Nb or V. The susceptibility of these dopants is modified considerably by their interactions

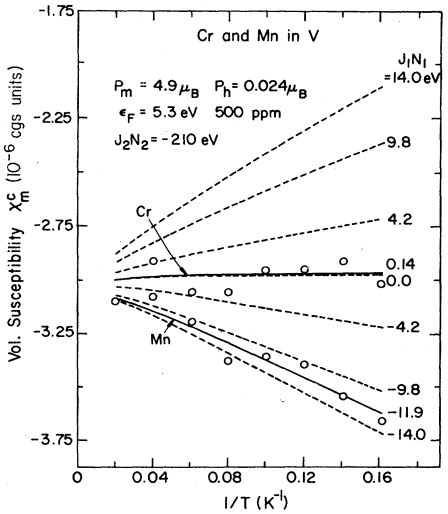

FIG. 6. Comparison of the susceptibility data with the results of the model calculation, for Cr and Mn dopants in V. The solid curves are plots of the calculated susceptibility $\chi_m^c(1/T)$ for Cr and Mn, and the circles represent the corresponding experimental values. Note that a negative value of J_1 accounts for the negative slope of the $\chi_m(1/T)$ data for Mn in V. The dashed curves are generated by using various values of J_1N_1.

with the conduction electrons and the host atoms. The effects of the dopant-host atom interaction are further illustrated by the dashed curves in Figs. 5 and 6, which are generated by using different values of J_1N_1, as shown.

We conclude from this analysis that localized moments are present on Cr and Mn dopant atoms in both Nb and V. We cannot establish the magnitudes of these moments on the basis of our results; it is, however, likely that these moments are much bigger than the values [Eqs. (2)—(5)] we obtained from the straightforward fits of χ_m to a Curie law.

B. Superconductivity measurements

We made superconductivity measurements on a total of 19 Nb samples. The measured characteristics of the pure samples are listed in Table II, and those of the doped samples are listed in Tables III and IV. We could not determine the lattice parameter of sample 17 reliably because it was so thin. The high T_c values for the pure samples are indicative of the high purity of our evaporated films [cf. $T_c = 9.23$ K for pure, bulk Nb (Ref. 30)]. The narrow transition widths δT_c for the pure as well as the doped samples show that the samples were homogeneous. The resistivity ratios (RR) vary from 3 to 10. That the resistivity ratios are low, despite high purity, may be an indication of a large degree of polycrystallinity in our samples. We found general trends towards higher RR and lower residual resistivity ρ with increasing film thickness d. Such trends have been seen previously for both evaporated[31–33] and sputtered[34] polycrystalline Nb films, and have been attributed to an increase of grain size with increasing film thickness.[34,35] Since scattering at grain boundaries contributes significantly to ρ,[35] an increase in the average grain size results in lower ρ and higher RR.

1. Transition temperature

Evident in Table II is a large scatter in the transition temperatures of the pure Nb samples. In order to discern the effects of the dopants on the transition temperature, we needed to determine the value of T_{c0} (the transition temperature in the absence of doping) for each doped sample. We found that the T_c's of the pure samples were linearly related to the lattice parameters a. This relation is shown in Fig. 7. (In addition to the data for the pure Nb films on which H_{c2} measurements were made, we have also included our measured values of T_c and a for three pure Nb films which were made for the susceptibility measurements, and two others.) The effect of the dopants on the transition temperature is also evident from Fig. 7. This figure enables us to assign a value of T_{c0} for each doped sample. The straight line in the figure is a least-squares fit to the pure Nb data. (Pure samples 6 and 10, which had abnormally small T_c's, have been excluded from the least-squares fit—this will be discussed later.) We use this straight-line fit and the measured value of a to obtain T_{c0} for each doped sample. The change in the transition temperature caused by the dopants, ΔT_c

TABLE II. Measured characteristics of the pure Nb samples used for the superconductivity measurements.

Sample no.	T_c (K)	δT_c (mK)	d (Å) ±1%	ρ ($\mu\Omega$ cm) ±2%	RR ±0.5%	a (Å) ±0.001 Å	$\left[\frac{-dH_{c2}}{dT}\right]$ at T_c (kG K^{-1}) ±2%
1	9.278	26	8818	2.78	6.95	3.2878	2.04
2	9.187	13	5656	3.57	6.11	3.2952	2.16
3	9.122	12	3760	2.33	8.56	3.3003	1.62
4	9.138	9	3766	4.46	5.18	3.3000	2.22
5	9.034	25	2595	6.20	3.99	3.3032	2.86
6	8.882	21	2388	6.88	3.88	3.3062	3.18
7	9.199	19	10231	3.59	6.01	3.2964	2.07
8	9.106	13	6780	3.19	7.07	3.3017	1.92
9	9.148	6	5160	2.68	7.44	3.2982	1.71
10	9.149	29	2081	4.57	4.64	3.2916	2.33
11	9.190	26	2672	4.22	5.01	3.2949	2.26
12	9.219	64	3313	3.72	5.82	3.2963	2.01

TABLE III. Measured characteristics of the doped samples used for the superconductivity measurements.

Sample no.	Dopant	T_c (K)	δT_c (mK)	d (Å) ±1%	ρ ($\mu\Omega$ cm) ±2%	RR ±0.5%	a (Å) ±0.001 Å	$\left[\frac{-dH_{c2}}{dT}\right]$ at T_c (kG K^{-1}) ±2%
13	Mn	9.087	19	2912	3.14	6.49	3.2976	1.97
14	Mn	8.978	34	3366	5.68	4.47	3.2983	2.53
15	Mn	9.028	25	2844	5.54	4.24	3.2930	2.74
16	Mn	9.245	23	3983	3.51	5.72	3.2854	2.00
17	Cr	8.954	16	1717	6.36	3.73		2.83
18	Cr	9.155	67	2922	5.33	3.95	3.2833	2.34
19	Cr	8.957	21	2835	6.88	3.57	3.2895	3.03

$=T_c-T_{c0}$, then follows, using our measured value of T_c for each doped sample. The values of T_{c0} and ΔT_c for the doped samples are listed in Table IV, along with the nominal dopant concentrations n_m.

Before ascribing the T_c depression caused by the dopants to the effects of magnetic pair breaking, we need to consider other mechanisms which could possibly lead to a decrease of the transition temperature of the doped samples:

(i) The Fermi level ϵ_F in Nb lies close to a sharp peak in the density of electronic states $g(\epsilon)$. A change Δn_e in the electron concentration caused by the presence of the dopants would move ϵ_F relative to this sharp peak in the density of electronic states, possibly resulting in a decrease of $g(\epsilon_F)$ and hence T_c for the doped sample. (We are using the rigid-band approximation.) To determine whether this effect is significant for our samples, we calculate the expected change in T_c caused by 300 ppm Cr, introduced interstitially in Nb. Assuming the maximum valence of 6 for the Cr dopants, we obtain $\Delta n_e=1.0\times10^{20}$ electrons cm^{-3} ($\Delta n_e/n_e=0.036\%$). The corresponding change in $g(\epsilon_F)$ is given by

$$\Delta g(\epsilon_F)\simeq\left[\frac{dg(\epsilon)}{d\epsilon}\right]_{\epsilon_F}\frac{d\epsilon_F}{dn_e}\Delta n_e=\frac{g'(\epsilon_F)}{2g(\epsilon_F)}\Delta n_e\ . \qquad (12)$$

Using estimates of $g'(\epsilon_F)$ and $g(\epsilon_F)$ from Ref. 24, we get $\Delta g(\epsilon_F)\simeq-0.88\times10^{32}$ states spin^{-1} erg^{-1} cm^{-3}. The decrease of T_c resulting from this change in $g(\epsilon_F)$ then follows from

$$\Delta T_c\simeq\frac{dT_c}{dg(\epsilon_F)}\Delta g(\epsilon_F)\ . \qquad (13)$$

To estimate $dT_c/dg(\epsilon_F)$ we write $dT_c/dg(\epsilon_F)=(dT_c/d\lambda)[d\lambda/dg(\epsilon_F)]$, where λ is the electron-phonon coupling constant. From Allen and Dynes's[36] modified version of McMillan's formula[37] for $T_c(\lambda)$, we get $dT_c/d\lambda=19.3$ K for Nb. Using the value $d\lambda/dg(\epsilon_F)\simeq0.035$ (10^{34} states spin^{-1} erg^{-1} cm^{-3})$^{-1}$ that we inferred for Nb from the calculation of Bennemann and Garland,[30] we obtain $dT_c/dg(\epsilon_F)\simeq0.68$ K (10^{34} states spin^{-1} erg^{-1} cm^{-3})$^{-1}$. We use this value in Eq. (13) to get $\Delta T_c=-0.006$ K, which shows that this effect is negligibly small for our samples.

(ii) A usual source of concern regarding evaporated Nb films is whether they accumulate gaseous contaminants during the deposition process. Oxygen is of particular concern, because Nb is a good getter of oxygen, and because oxygen (when present interstitially) has a marked effect on the superconducting properties of Nb.[38,39] Koch *et al.*[39] found that the addition of oxygen interstitially to Nb increased the lattice parameter at a rate of 0.0039 Å/at. % O, and changed T_c at a rate of -0.93 K/at. % O. If caused by interstitial oxygen, the total variation of a in our pure films would correspond to 4.6 at. % O, which in turn should result in a T_c change of 4.28 K—greater than our observed variation by a factor of 14. Besides, an oxygen concentration of 4.6 at. % is higher than the solubility limit.[40] This shows that our pure Nb films do not contain appreciable amounts of interstitial oxygen.

TABLE IV. T_c depression, $\Delta T_c=T_c-T_{c0}$, caused Cr and Mn dopants in Nb.

Sample no.	Constituents	n_m (ppm)	T_{c0} (K) (calc.)	ΔT_c (K) ±10%
13	Nb-Mn	500	9.153	−0.066
14	Nb-Mn	300	9.142	−0.164
15	Nb-Mn	300	9.224	−0.196
16	Nb-Mn	600	9.343	−0.098
17	Nb-Cr	300		
18	Nb-Cr	300	9.375	−0.220
19	Nb-Cr	300	9.279	−0.322

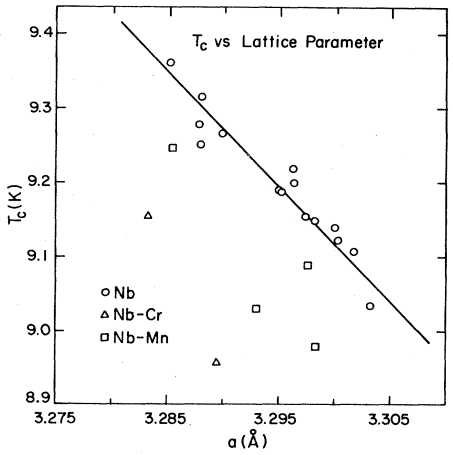

FIG. 7. Variation of the transition temperature with lattice parameter a. The straight line is a least-squares fit to the pure Nb data. The depression of the transition temperature caused by Cr and Mn dopants is evident.

Since the doped films were deposited under the same conditions as the pure films, we believe that they do not contain interstitial oxygen either. The T_c depression in our doped samples cannot, therefore, be the result of an oxygen-related effect. We conclude that oxygen does not play a significant role in controlling the T_c of our pure and doped samples. Possible exceptions to this rule are samples 6 and 10, whose T_c's were abnormally low compared to those of the other pure samples. During the deposition of each of these samples, the ratio of the background pressure to the deposition rate was relatively high, so some interstitial oxygen could have been introduced.

We conclude that the T_c depression caused by the dopants should be attributed to the effects of magnetic pair breaking. This conclusion is consistent with the results of our susceptibility measurements, which provided evidence for the presence of a localized moment (and hence, a localized spin) on each Cr and Mn dopant atom in Nb. We will now discuss our results for ΔT_c in further detail.

It is clear from Table IV that the values of ΔT_c do not correlate with n_m—this is not surprising in view of the uncertainties in the nominal concentrations. In order to obtain a meaningful estimate for $-dT_c/dn_m$, the rate of depression of T_c with dopant concentration, we first note that the normalized T_c depressions, $-\Delta T_c/T_{c0}$, are small, ranging from 0.007 to 0.035. In this range, ΔT_c is expected to be proportional to n_m:[11,41,42] We can therefore derive an average value of $-dT_c/dn_m$ for our samples from

$$-\left[\frac{dT_c}{dn_m}\right]_{\rm av}=-\frac{1}{N}\sum\frac{\Delta T_c}{n_m}\ , \tag{14}$$

where the sum is taken over samples 18 and 19 for Cr dopants, and over samples 13 to 16 for Mn dopants. We obtain

$$-\frac{dT_c}{dn_m}=\begin{cases}9.03\ \text{K/at. \% for Cr}\ ,\\ 3.74\ \text{K/at. \% for Mn}\ .\end{cases} \tag{15}$$

These values are not inconsistent with the band calculations of Kunz and Ginsberg[13] for Cr and Mn dopants in Nb. By including the effects of $l=1$ and 2 partial waves in Shiba's theory, they obtained $-dT_c/dn_m=14.5$ K/at. % for Cr in the $3d^5 4s$ atomic configuration, with spin $S=3$. For Mn, they obtained $-dT_c/dn_m=4.96$ K/at. %, for the $3d^7$ configuration with $S=\frac{3}{2}$.

From our estimate of $-dT_c/dn_m$, we can also calculate values of the critical concentration $n_{\rm cr}$ for Cr and Mn dopants in Nb. From Refs. 11 or 41 we have

$$-\frac{dT_c}{dn_m}=\frac{0.691T_{c0}}{n_{\rm cr}}\ . \tag{16}$$

Using average values of T_{c0} for the Cr- and Mn-doped samples, respectively, we get

$$n_{\rm cr}=\begin{cases}0.714\ \text{at. \% for Cr},\\ 1.70\ \text{at. \% for Mn}.\end{cases} \tag{17}$$

It is clear from the results in Eqs. (15) and (17) that Cr has a much larger effect on the superconductivity of Nb than does Mn. This could be the result of a higher spin associated with each Cr dopant atom. It could also arise from a stronger exchange constant for the interaction between the dopants and the conduction electrons for Cr dopants as compared to Mn.

2. *Upper critical field*

The critical-field data, $H_{c2}(T)$, for one of our samples (sample 12, a pure Nb film) are shown in Fig. 8. The $H_{c2}(T)$ curve in this figure is representative: The $H_{c2}(T)$ curves for all our samples show the same characteristic behavior—they are linear near T_c ($0.9\lesssim T/T_c\leq 1$) and then exhibit a positive curvature at slightly lower temperatures. Such positive curvature in $H_{c2}(T)$ has been seen previously for Nb films (see, for example, Refs. 31, 33, and 34) as well as for bulk samples,[43] and has been interpreted as resulting from sample inhomogeneities[33] or

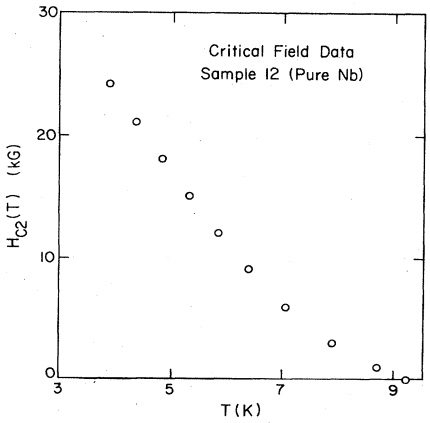

FIG. 8. Critical-field data, $H_{c2}(T)$, for sample 12, a pure Nb film.

from anisotropy of the Fermi surface.[43] In order to determine whether this effect could result from possible inhomogeneities at the edges of the films, we scribed the edges of some of our films away from the middle and repeated the measurements. We found[6] that the scribing did not change the shape of the critical-field curves. The observed shape may result from anisotropy of the Fermi surface.[44,45]

The positive curvature in our $H_{c2}(T)$ curves is sample dependent, which precludes a quantitative assessment of the effects of the magnetic dopants on the critical field. On a qualitative level, however, we can compare our results for $H_{c2}(T)$ with predictions of the theory of Fulde and Maki[18] by considering averages of the suitably normalized critical-field curves. If the values of H_{c2} are normalized to $-dH_{c2}/dT$ at T_c or to $1/D$, where D is the electron diffusion constant, additive pair breaking would be indicated by H_{c2}-vs-T curves which are shifted downward by doping, without changing shape. Figure 9 shows the averages of the $H_{c2}(T)$ curves for the pure, Cr-doped, and Mn-doped samples respectively, as a function of T/T_{c0}. The curves are normalized to our measured values of $(-dH_{c2}/dT)_{T_c}$. The averaging is done by first computing a spline fit to the measured values of $H_{c2}/(-dH_{c2}/dT)_{T_c}$ for each sample, and then using these spline fits to calculate the average of the normalized critical fields at various values of T/T_{c0}. Figure 10 shows the averages of the $H_{c2}(T)$ curves normalized using $1/D$, where D is obtained from $D=\frac{1}{3}v_F^*l$, in which v_F^* is the electron-phonon renormalized Fermi velocity, and l is the mean free path. [The values of v_F^* and l, for each sample, were estimated[6] from our measured values of T_c, ρ, and $(-dH_{c2}/dT)_{T_c}$, using results[46] from the Ginzburg-Landau-Abrikosov-Gorkov theory of type-II superconductivity, including corrections for the electron-phonon interaction.]

It can be seen from Figs. 9 and 10 that the critical-field curves for the doped samples are shifted downward from those for the pure samples. Also, the curves in each figure show the same qualitative behavior as a function of

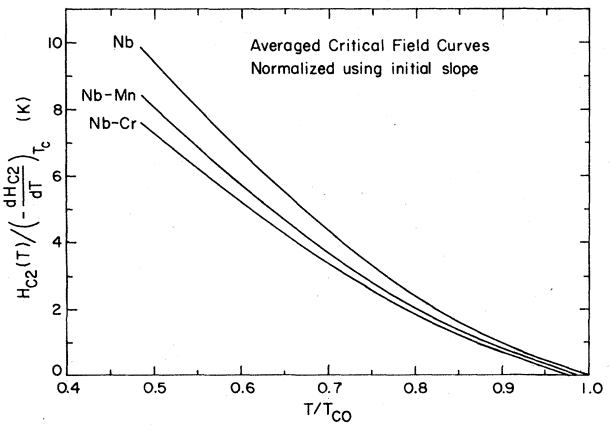

FIG. 9. Averages of the normalized $H_{c2}(T)$ curves, plotted against T/T_{c0}. Measured values of $-dH_{c2}/dT$ at $T=T_c$ have been used as normalizing parameters. The averaging procedure is described in the text.

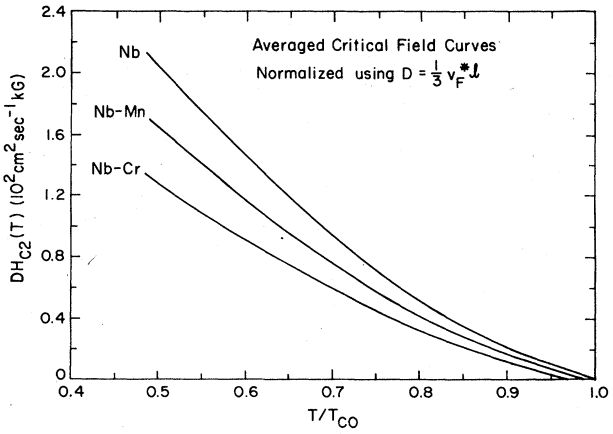

FIG. 10. Averages of the normalized $H_{c2}(T)$ curves, plotted against T/T_{c0}. Calculated values of $1/D$, where $D=\frac{1}{3}v_F^*l$, have been used as normalizing parameters. The averaging procedure is described in the text.

decreasing $t=T/T_{c0}$: They are linear and coparallel until $t\simeq 0.9$, and then progressively diverge from each other with decreasing temperature. In view of the different behavior in these two temperature regions, we will consider each region separately, using the notation $H_{\mathrm{Nb}}(t)$, $H_{\mathrm{Cr}}(t)$, and $H_{\mathrm{Mn}}(t)$ to denote the averaged critical-field curves for the pure, Cr-doped, and Mn-doped samples respectively.

(i) In the high-temperature region $t\gtrsim 0.9$, both $H_{\mathrm{Nb}}(t)-H_{\mathrm{Cr}}(t)$ and $H_{\mathrm{Nb}}(t)-H_{\mathrm{Mn}}(t)$ are positive and independent of temperature. This indicates that the pair-breaking effects of the dopants and of the applied field are additive, and that the pair-breaking effect of the dopants is independent of temperature, in accordance with the theory of Fulde and Maki.[18]

(ii) In the lower-temperature region, $t\lesssim 0.9$, although both $H_{\mathrm{Nb}}(t)$-$H_{\mathrm{Cr}}(t)$ and $H_{\mathrm{Nb}}(t)$-$H_{\mathrm{Mn}}(t)$ are positive, they are not independent of temperature. If this temperature dependence is caused by effects of the magnetic dopants, it implies a temperature-dependent pair-breaking parameter, which could result from alignment of the dopant spins in the applied field.[47] However, this temperature dependence could also arise from the same mechanism that leads to positive curvature of the critical-field curves. We find[6] that the magnitude of the positive-curvature effect in our samples tends to increase with decreasing resistivity and increasing film thickness. The pure samples (with generally lower resistivities and higher thicknesses) tend to have larger positive curvatures than do the doped samples. This trend could account for the increase in $H_{\mathrm{Nb}}(t)$-$H_{\mathrm{Cr}}(t)$ and $H_{\mathrm{Nb}}(t)$-$H_{\mathrm{Mn}}(t)$ with decreasing t. Since the Mn-doped samples have generally lower resistivities and higher thicknesses than the Cr-doped samples, the same argument can explain the increase in $H_{\mathrm{Mn}}(t)$-$H_{\mathrm{Cr}}(t)$ with decreasing t that can be seen in each figure. Finally, we note that the curves in Figs. 9 and 10 start to diverge from each other at $t\simeq 0.9$, about the same temperature at which the positive curvature starts, so that, if

the divergence arises purely as a result of the positive-curvature effect, the pair breaking caused by the magnetic dopants is independent of temperature.

We conclude, for both Cr and Mn dopants in Nb, that (a) the pair-breaking effects of the dopants and of the applied field are additive near T_c; (b) the apparent temperature dependence of the pair-breaking effect of the dopants at lower temperatures is possibly a result of the resistivity-dependent and thickness-dependent differential positive curvature between the critical-field curves of the pure and doped samples, and not a result of dopant spin alignment; and (c) it is thus possible that the pair-breaking effect of the dopants is independent of temperature.

ACKNOWLEDGMENTS

We thank Professor C. P. Slichter for very useful suggestions regarding the analysis of the susceptibility data. This research was supported by the National Science Foundation under Grant No. DMR-82-03528.

*Present address: Los Alamos National Laboratory, Los Alamos, NM 87545.

[1]J. Friedel, Can. J. Phys. **34**, 1190 (1956); Nuovo Cimento (Suppl.) **7**, 287 (1958).
[2]P. W. Anderson, Phys. Rev. **124**, 41 (1961).
[3]P. A. Wolff, Phys. Rev. **124**, 1030 (1961).
[4]J. R. Schrieffer, J. Appl. Phys. **38**, 1143 (1967).
[5]D. K. Wohlleben and B. R. Coles, in *Magnetism,* edited by H. Suhl (Academic, New York, 1973), Vol. V, p. 3.
[6]A. Roy, Ph.D. thesis, University of Illinois at Urbana—Champaign, 1984 (unpublished).
[7]A. J. Heeger, in *Solid State Physics,* edited by F. Seitz, D. Turnbull, and H. Ehrenreich (Academic, New York, 1969), Vol. 23, p. 283.
[8]M. D. Daybell and W. A. Steyert, Rev. Mod. Phys. **40**, 380 (1968).
[9]A. Blandin, in *Magnetism,* Ref. 5, p. 57.
[10]J. L. Smith and E. A. Kmetko, J. Less-Common Metals **90**, 83 (1983).
[11]H. Shiba, Prog. Theor. Phys. **40**, 435 (1968).
[12]E. Müller-Hartmann, in *Magnetism,* Ref. 5, p. 353.
[13]A. B. Kunz and D. M. Ginsberg, Phys. Rev. B **22**, 3165 (1980).
[14]D. S. Buchanan, A. Roy, D. M. Ginsberg, and J. E. Cunningham, Phys. Rev. B **29**, 2469 (1984).
[15]E. E. Barton and H. Claus, Phys. Rev. B **1**, 3741 (1970).
[16]J. Müller, Helv. Physica Acta **32**, 141 (1959).
[17]G. Gladstone, M. A. Jensen, and J. R. Schrieffer, in *Superconductivity,* edited by R. D. Parks (Marcell Dekker, New York, 1969), p. 665.
[18]P. Fulde and K. Maki, Phys. Rev. **141**, 275 (1966).
[19]D. S. Buchanan, Ph.D. thesis, University of Illinois at Urbana—Champaign, 1983 (unpublished).
[20]VTS-50 SQUID Susceptometer made by S.H.E. Corporation, San Diego, CA 92121.
[21]A. Roy *et al.* (unpublished).
[22]E. C. Stoner, Philos. Mag. **36**, 803 (1945).
[23]*American Institute of Physics Handbook,* 3rd ed. (AIP, New York, 1972).
[24]L. F. Mattheiss, Phys. Rev. B **1**, 373 (1970).
[25]D. A. Papaconstantopoulos, J. R. Anderson, and J. W. McCaffrey, Phys. Rev. B **5**, 1214 (1972).
[26]E. C. Stoner, Proc. R. Soc. London, Ser. A **154**, 656 (1936); see also Ref. 29, p. 669.
[27]D. M. Burnell, J. Zasadzinski, R. J. Noer, E. L. Wolf, and G. B. Arnold, Solid State Commun. **41**, 637 (1982).
[28]G. C. Carter, L. H. Bennett, and D. J. Kahan, Prog. Mater. Sci. **20**, (1977).
[29]N. W. Ashcroft and N. P. Mermin, *Solid State Physics* (Holt, Rinehart and Winston, New York, 1976), p. 38.
[30]K. H. Bennemann and J. W. Garland, in *Superconductivity in d- and f-Band Metals,* edited by D. H. Douglass (AIP, New York, 1972), p. 103.
[31]Y. Asada and H. Nose, J. Phys. Soc. Jpn. **26**, 347 (1969).
[32]O. G. Vendik, M. M. Gaidukov, A. B. Kozyrev, N. F. Leont'eva, E. G. Pavlyuk, N. A. Potsar, and T. B. Samoilova, Fiz. Tverd. Tela **21**, 3279 (1979) [Sov. Phys.—Solid State **21**, 1893 (1980)].
[33]V. M. Pan, V. G. Prokhorov, and G. G. Kaminskii, Sov. J. Low Temp. Phys. **6**, 470 (1980).
[34]J. J. Hauser and H. C. Theurer, Phys. Rev. **134**, A198 (1964).
[35]A. F. Mayadas and M. Shatzkes, Phys. Rev. B **1**, 1382 (1970).
[36]P. B. Allen and R. C. Dynes, Phys. Rev. B **12**, 905 (1975).
[37]W. L. McMillan, Phys. Rev. **167**, 331 (1968).
[38]W. DeSorbo, Phys. Rev. **132**, 107 (1963).
[39]C. C. Koch, J. O. Scarbrough, and D. M. Kroeger, Phys. Rev. B **9**, 888 (1974).
[40]A. U. Seybolt, Trans. AIME **200**, 774 (1954).
[41]A. A. Abrikosov and L. P. Gor'kov, Zh. Eksp. Teor. Fiz. **39**, 1781 (1960) [Sov. Phys.—JETP **12**, 1243 (1961)].
[42]M. B. Maple, in *Magnetism,* Ref. 5, p. 289.
[43]S. J. Williamson, Phys. Rev. B **2**, 3545 (1970).
[44]P. C. Hohenberg and N. R. Werthamer, Phys. Rev. **153**, 493 (1967).
[45]P. Entel and M. Peter, J. Low Temp. Phys. **22**, 613 (1976).
[46]T. P. Orlando, E. J. McNiff, Jr., S. Foner, and M. R. Beasley, Phys. Rev. B **19**, 4545 (1979).
[47]O. Fischer and M. Peter, in *Magnetism,* Ref. 5, p. 327.